J|A|C|S
ARTICLES
Published on Web 08/10/2004

In Vitro Demonstration of the Heavy-Atom Effect for Photodynamic Therapy

Aoife Gorman,[†] John Killoran,[†] Caroline O'Shea,[‡] Tony Kenna,[‡] William M. Gallagher,[‡] and Donal F. O'Shea*,[†]

Contribution from the Centre for Synthesis and Chemical Biology, Conway Institute of Biomolecular and Biomedical Research, Department of Chemistry and Department of Pharmacology, University College Dublin, Belfield, Dublin 4, Ireland

Received April 23, 2004; Revised Manuscript Received June 11, 2004; E-mail: donal.f.oshea@ucd.ie

Abstract: Photodynamic therapy (PDT) is an emerging treatment modality for a range of disease classes, both cancerous and noncancerous. This has brought about an active pursuit of new PDT agents that can be optimized for the unique set of photophysical characteristics that are required for a successful clinical agent. We now describe a totally new class of PDT agent, the BF_2-chelated 3,5-diaryl-1*H*-pyrrol-2-yl-3,5-diarylpyrrol-2-ylideneamines (tetraarylazadipyrromethenes). Optimized synthetic procedures have been developed to facilitate the generation of an array of specifically substituted derivatives to demonstrate how control of key therapeutic parameters such as wavelength of maximum absorbance and singlet-oxygen generation can be achieved. Photosensitizer absorption maxima can be varied within the body's therapeutic window between 650 and 700 nm, with high extinction coefficients ranging from 75 000 to 85 000 M^{-1} cm^{-1}. Photosensitizer singlet-oxygen generation level was modulated by the exploitation of the heavy-atom effect. An array of photosensitizers with and without bromine atom substituents gave rise to a series of compounds with varying singlet-oxygen generation profiles. X-ray structural evidence indicates that the substitution of the bromine atoms has not caused a planarity distortion of the photosensitizer. Comparative singlet-oxygen production levels of each photosensitizer versus two standards demonstrated a modulating effect on singlet-oxygen generation depending upon substituent patterns about the photosensitizer. Confocal laser scanning microscopy imaging of **18a** in HeLa cervical carcinoma cells proved that the photosensitizer was exclusively localized to the cellular cytoplasm. In vitro light-induced toxicity assays in HeLa cervical carcinoma and MRC5-SV40 transformed fibroblast cancer cell lines confirmed that the heavy-atom effect is viable in a live cellular system and that it can be exploited to modulate assay efficacy. Direct comparison of the efficacy of the photosensitizers **18b** and **19b**, which only differ in molecular structure by the presence of two bromine atoms, illustrated an increase in efficacy of more than a 1000-fold in both cell lines. All photosensitizers have very low to nondeterminable dark toxicity in our assay system.

Introduction

Photodynamic therapy (PDT) is a noninvasive technique for the treatment of a variety of cancer tumor types by the combined use of visible or near-visible light with a photosensitizing drug.[1] The therapeutic strategy is as follows: a photosensitizer of minimal dark toxicity is introduced into the body, which accumulates to some extent preferentially within the tumor. The tumor is then selectivity irradiated with low-energy light of wavelength that can pass through the body's therapeutic window (650−900 nm), resulting in excitation of the photosensitizer. The light-activated photosensitizer then transfers its excited-state energy to surrounding biological tissue via singlet oxygen, resulting in oxidative cellular damage, leading to cell death via apoptosis and/or necrosis.[2] The photosensitizer returns to its ground state and the process can repeat as long as the light source remains and molecular oxygen is present. After light treatment, the photosensitizer is allowed to clear from the body and the treatment is complete. Due to the short half-life (0.6×10^{-6} s) and diffusion distance (0.1 μm) of singlet oxygen in aqueous media, PDT can be considered a highly selective form of cancer treatment, as only the irradiated areas are affected, provided that the photosensitizer is nontoxic in the absence of light.[3] This combination of light/photosensitizer/oxygen as a mode of disease treatment has expanded from an initial focus on cancer tumors to include application in certain nonneoplastic diseases including age-related macular degeneration (AMD),[4] coronary heart disease,[5] periodontal diseases,[6] and microbial infections.[7]

[†] Department of Chemistry.
[‡] Department of Pharmacology.

(1) For recent reviews, see: (a) Dolmans, D. E. J. G. J.; Fukumura, D.; Jain, R. K. *Nature Reviews Cancer* **2003**, *3*, 380. (b) MacDonald, I. J.; Dougherty, T. J. *J. Porphyrins Phthalocyanines* **2001**, *5*, 105. (c) Sharman, W. M.; Allen, C. M.; van Lier, J. E. *Drug Discovery Today* **1999**, *4*, 507. (d) Dougherty, T. J.; Gomer, C. J.; Henderson, B. W.; Jori, G.; Kessel, D.; Korbelik, M.; Moan, J.; Peng, Q. *J. Natl. Cancer Inst.* **1998**, *90*, 889. (e) Bonnett, R. *Chem. Soc. Rev.* **1995**, *24*, 19.

(2) Oleinick, N. L.; Morris, R. L.; Belichenko, I. *Photochem. Photobiol. Sci.* **2002**, *1*, 1.

(3) Henderson, B. W.; Dougherty, T. J. *Photochem. Photobiol.* **1992**, *55*, 145.

10.1021/ja047649e CCC: $27.50

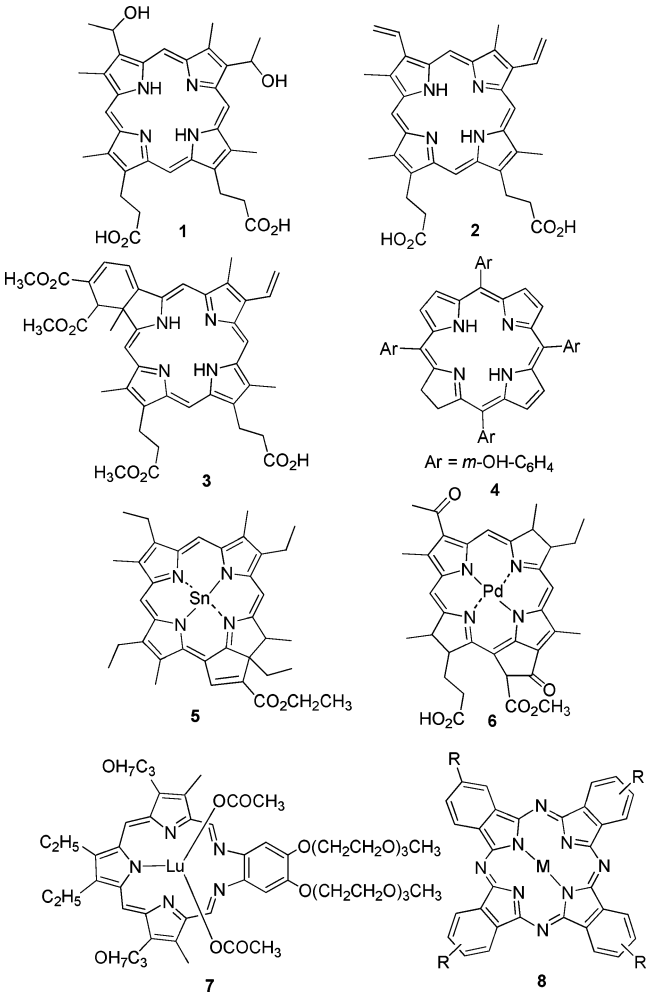

Figure 1. Polypyrrole macrocyclic PDT agents.

Photofrin was the first, and at the present time remains the most common, clinically used PDT agent. Although it has been approved for use in the United States, Canada, Japan, and Europe for the treatment of esophageal, endobroncheal, bladder, lung, stomach, cervical, and skin cancers,[1b] it is widely recognized that it is far from being an ideal drug for use in PDT.[8] It is an undefined mixture of dimeric and oligomeric compounds derived from the acidic treatment of hematoporphyrin **1** followed by a semipurification (Figure 1). Over the past 20 years attempts to develop alternatives to Photofrin have predominantly focused on various types of polypyrrole macrocycles generally termed second-generation PDT agents. Examples from the porphyrin class are protoporphyrin IX **2**, which therapeutically is administered as its biosynthetic precursor, 5-aminolevulinic acid, for the treatment of Barrett's esophagus and skin cancers.[9] The benzoporphyrin derivative **3** (Visudyne) is widely used for the treatment of AMD.[4] Examples from the dihydroporphyrin or chlorin class are *m*-tetrahydroxyphenylchlorin **4** (Foscan), which has gained regulatory approval in Europe for the treatment of head and neck cancer,[10] and tin etiopurpurin (Purlytin) **5**, which is in a clinical trial for the treatment of AMD.[11] The palladium-bacteriopheophorbide **6** (TOOKAD),[12] the expanded porphyrin **7** (Motexafin Lutetium),[13] and the phthalocyanines[14] **8** are all in various stages of clinical trials for a number of cancerous tissue targets.

The investigation of non-porphyrin photosensitizers for the development of novel PDT agents has been considerably less extensive.[15] To date, the focus has been primarily on the cationic photosensitizers such as methylene blue **9**,[16] nile blue analogue **10**,[17] and the chalcogenopyrylium class of sensitizer **11**[18] (Figure 2). Significant drawbacks of these classes appear to be their high inherent dark toxicity, perhaps due to the nuclear localization of these cationic compounds, and their relatively short absorption maxima of less than 650 nm in aqueous solutions.[16b,c,17a,18d] Even though many of the nonporphyrinic PDT agents investigated predate the development of second-generation photosensitizers, none have been approved for use in vivo. The most successful has been methylene blue **9**, which is used ex vivo for the inactivation of extracellular enveloped viruses in blood plasma.[19]

Despite its achievements, PDT remains in its developmental stages with a marked need to progress alternative photosensi-

(4) Hooper, C. Y.; Guymer, R. H. *Clin. Exp. Ophthalmol.* **2003**, *31*, 376 (review).
(5) (a) Kereiakes, D. J.; Szyniszewski, A. M.; Wahr, D.; Herrmann, H. C.; Simon, D. I.; Rogers, C.; Kramer, P.; Shear, W.; Yeung, A. C.; Shunk, K. A.; Chou, T. M.; Popma, J.; Fitzgerald, P.; Carroll, T. E.; Forer, D.; Adelman, D. C. *Circulation* **2003**, *108*, 1310. (b) Hayase, M.; Woodbum, K. W.; Perlroth, J.; Miller, R. A.; Baumgardner, W.; Yock, P. G.; Yeung, A. *Cardiovascular Res.* **2001**, *49*, 449. (c) Mansfield, R.; Bown, S.; McEwan, J. *Heart* **2001**, *86*, 612 (review).
(6) (a) Kömerik, N.; Nakanishi, H.; MacRobert, A. J.; Henderson, B.; Speight, P.; Wilson, M. *Antimicrob. Agents Chemother.* **2003**, *47*, 932. (b) Kömerik, N.; Wilson, M. *J. Appl. Microbiol.* **2002**, *92*, 618. (c) Wilson, M. *J. Appl. Bacteriol.* **1993**, *75*, 299.
(7) (a) Hamblin, M. R.; Zahra, T.; Contag, C. H.; McManus, A. T.; Hasan, T. *J. Infect. Diseases* **2003**, *187*, 1717. (b) Romanova, N. A.; Brovko, L. Y.; Moore, L.; Pometun, E.; Savitsky, A. P.; Ugarova, N. N.; Griffiths, M. W. *Appl. Environ. Microbiol.* **2003**, *69*, 6393. (c) Hamblin, M. R.; O'Donnell, D. A.; Murthy, N.; Contag, C. H.; Hasan, T. *Photochem. Photobiol.* **2002**, *75*, 51.
(8) Ochsner, M. *Drug Res.* **1997**, *47*, 1185.
(9) (a) Overholt, B. F.; Panjehpour, M.; Halberg, D. L. *Gastrointestinal Endoscopy* **2003**, *58*, 183. (b) Gossner, L.; Stolte, M.; Sroka, R.; Rick, K.; May, A.; Hahn, E. G.; Ell, C. *Gastroenterology* **1998**, *114*, 448. (c) Barr, H.; Shepherd, N. A.; Dix, A.; Roberts D. J. H.; Tan, W. C.; Krasner, N. *Lancet* **1996**, *348*, 584.
(10) (a) Copper, M. P.; Bing Tan, I.; Oppelaar, H.; Ruevekamp, M. C.; Stewart, F. A. *Arch. Otolaryngol.* **2003**, *129*, 709. (b) Fan, K. F. M.; Hopper, C.; Speight, P. M.; Buonaccorsi, G. A.; Bown, S. G. *Int. J. Cancer* **1997**, *73*, 25.
(11) Mang, T. S.; Allison, R.; Hewson, G.; Snider, W.; Moskowitz, R. *Cancer J. Sci. Am.* **1998**, *4*, 378.
(12) (a) Koudinova, N. V.; Pinthus, J. H.; Brandis, A.; Brenner, O.; Bendel, P.; Ramon, J.; Eshhar, Z.; Scherz, A.; Salomon, Y. *Int. J. Cancer* **2003**, *104*, 782. (b) Chen, Q.; Huang, Z.; Luck, D.; Beckers, J.; Brun, P. H.; Wilson, B. C.; Scherz, A.; Salomon, Y.; Hetzel, F. W. *Photochem. Photobiol.* **2002**, *76*, 438.
(13) Sessler, J. L.; Miller, R. A. *Biochem. Pharmacol.* **2000**, *59*, 733 (review).
(14) (a) Bench, B. A.; Beveridge, A.; Sharman, W. M.; Diebold, G. J.; van Lier J. E.; Gorun, S. M. *Angew. Chem., Int. Ed.* **2002**, *41*, 748. (b) Ball, D. J.; Mayhew, S.; Wood, S. R.; Griffiths, J.; Vernon, D. I.; Brown, S. B. *Photochem. Photobiol.* **1999**, *69*, 390. (c) Hu, M.; Brasseur, N.; Yildiz, S. Z.; van Lier, J. E.; Leznoff, C. C. *J. Med. Chem.* **1998**, *41*, 1789. (d) Allemann, E.; Brasseur, N.; Kudrevich, S. V.; La Madeleine, C.; van Lier, J. E. *Int. J. Cancer* **1997**, *72*, 289.
(15) Wainwright, M. *Chem. Soc. Rev.* **1996**, 351 (review).
(16) (a) Wainwright, M.; Crossley, K. B. *J. Chemother.* **2002**, *14*, 431 (review). (b) Mellish, K. J.; Cox, R. D.; Vernon, D. I.; Griffiths, J.; Brown, S. B. *Photochem. Photobiol.* **2002**, *75*, 392. (c) Wainwright, M.; Phoenix, D. A.; Rice, L.; Burrow, S. M.; Waring, J. *J. Photochem. Photobiol. B* **1997**, *40*, 233. (d) Orth, K.; Ruck, A.; Stanescu, A.; Berger, H. G. *Lancet* **1995**, *345*, 519.
(17) (a) Tong, Z.; Singh, G.; Rainbow, A. J. *Photochem. Photobiol.* **2001**, *74*, 707. (b) Frimberger, A. E.; Moore, A. S.; Cincotta, L.; Cotter, S. M.; Foley, J. R. *Clinical Cancer Res.* **1944**, *4*, 2207. (c) Cincotta, L.; Foley, J. W.; Maceachern, T.; Lampros, E.; Cincotta, A. H. *Cancer Res.* **1994**, *54*, 1249.
(18) (a) Detty, M. R.; Merkel, P. B. *J Am. Chem. Soc.* **1990**, *112*, 3845. (b) Leonard, K. A.; Nelen, M. I.; Anderson, L. T.; Gibson, S. L.; Hilf, R.; Detty, M. R. *J. Med. Chem.* **1999**, *42*, 3942. (c) Leonard, K. A.; Hall, J. P.; Nelen, M. I.; Davies, S. R.; Gollnick, S. O.; Camacho, S.; Oseroff, A. R.; Gibson, S. L.; Hilf, R.; Detty, M. R. *J. Med. Chem.* **2000**, *43*, 4488. (d) Brennan N. K.; Hall, J. P.; Davies, S. R.; Gollnick, S. O.; Oseroff, A. R.; Gibson, S. L.; Hilf, R.; Detty, M. R. *J. Med. Chem.* **2002**, *45*, 5123.
(19) (a) Williamson, L. M.; Cardigan, R.; Prowse, C. V. *Transfusion* **2003**, *43*, 1322 (review). (b) Jockusch, S.; Lee, D.; Turro, N. J.; Leonard, E. F. *Proc. Natl. Acad. Sci. U.S.A.* **1996**, *93*, 7446.

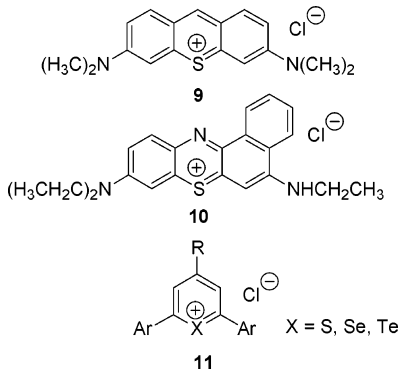

Figure 2. Non-porphyrin PDT agents.

tizers with improved efficacy and side effect profiles. To further advance this novel form of treatment, it has become apparent that the development of new PDT compounds is needed, together with a more thorough and integrated understanding of the multitude of targets/actions so far ascribed to PDT. New PDT agents have largely come from the class of polypyrrole macrocycles. As a class of compound they have, to varying degrees, many of the inherent photophysical properties that would be required for a successful PDT agent, such as cancer tissue localization, therapeutic window absorption, and capacity for singlet-oxygen generation. The drawbacks associated with this class of compound can be their challenging synthesis and purification, which can restrict the fine-tuning of their photophysical and biological properties.

As a result of the rapidly increasing number of divergent therapeutic targets ascribed to PDT, it has become imperative that new classes of agents be explored. Our approach was to develop a completely new structural platform from which a sequentially modified array of PDT agents could be developed. This would facilitate the refinement of the essential therapeutic parameters of a PDT agent to match the specific therapeutic target of choice by straightforward functional group manipulation of a core photosensitizer scaffold. To achieve this goal it would be essential to develop a robust synthetic route to our scaffold that would enable us to incorporate specific functional groups either before or after scaffold synthesis, which in turn would allow for optimization of the photophysical and biological properties necessary for a successful therapeutic agent.

PDT agents have an atypical mode by which their efficacy can be optimized. Conventional therapeutics, which operate through modes of action such as enzyme inhibition or receptor interaction, are often discovered by a structure-based design approach, centered upon molecular features such as 3-D binding, electrostatic, hydrophobic, and hydrogen-bonding interactions of the drug with the site of interaction. In contrast, the efficacy of a PDT agent can be governed by three factors: (i) the photosensitizer localization, (ii) the extent of light activation of the photosensitizer in vivo, and (iii) the efficiency of an intersystem crossing (ISC) from the first excited singlet state to the triplet state of the photosensitizer (Figure 3).

To have two photochemical processes (absorption and ISC) as pivotal controlling points determining a treatment efficacy is completely unique to this mode of therapy. Thus, any approach to influence the therapeutic effectiveness by exerting direct control over these processes warrants investigation.

It would be advantageous to have control over absorbance wavelength, as it could be envisaged that different tissue types

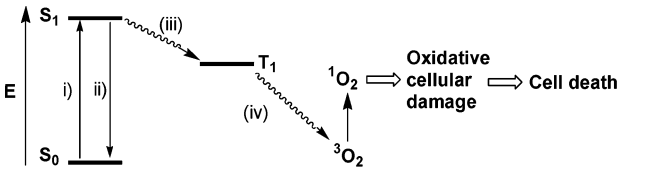

Figure 3. Simplified Jablonski diagram for the PDT process.

would require different excitation wavelengths dependent upon tissue location (deep-seated tumors versus skin lesions), size, density, and pigmentation. The depth of light penetration through tissue is directly related to wavelength;[20] thus, if an array of photosensitizers could be generated containing only minor peripheral structural modifications, which had different maxima of absorption, this would allow for the matching of a specific PDT agent to tissue type.

As singlet oxygen is the key cytotoxic agent in the PDT therapeutic process, it is essential that control can be exerted over this component of the therapy. The quantity of singlet oxygen generated by a photosensitizer is regulated by the efficiency of a spin-forbidden electronic transition from a singlet to a triplet state (ISC). The introduction of a heavy atom into a molecule is known to have an influence over the rates of the ISC and is termed the heavy-atom effect.[21] The ability to synthetically incorporate a heavy atom within the photosensitizer could be a mechanism for exerting the desired control over levels of singlet-oxygen generation. It would be of significant clinical benefit if a range of photosensitizers were available with programmed levels of singlet oxygen production capability that only differed in chemical structure by minor peripheral modifications to a single core photosensitizer. This could facilitate the building of an array of varying singlet oxygen producers to suit different therapeutic needs and profiles.

Herein we will show how we can exert control over several key stages of a PDT process by the judicious positioning of substituents around a common photosensitizer scaffold. The goals of this work were to determine the peripheral substitution patterns that would facilitate a stepwise bathochromatic shift of absorption maximum from 650 to 700 nm and deliver incremental controlled singlet oxygen production levels for an array of photosensitizers all constructed from a common scaffold. These compounds would then be tested in vitro to determine if our controls would be viable in a living cellular system.

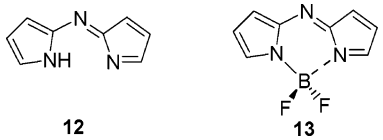

Figure 4. Azadipyrromethenes.

Our starting point was a neglected class of chromophore, the azadipyrromethenes **12** (Figure 4). These compounds were first described in the 1940s and have remained unstudied for any application since that time.[22] As compounds of type **12** are not macrocyclic, we anticipated that it would be necessary to convert

(20) Wilson, B. C.; Patterson, M. S.; Lilge, L. *Lasers Med. Sci*. **1997**, *12*, 182 (review).
(21) Turro, N. J. In *Modern Molecular Photochemistry*; University Science Books: Sausalito, CA, 1991; pp 191−195.
(22) Rogers, M. A. T. *J. Chem. Soc.* **1943**, 596.

Scheme 1

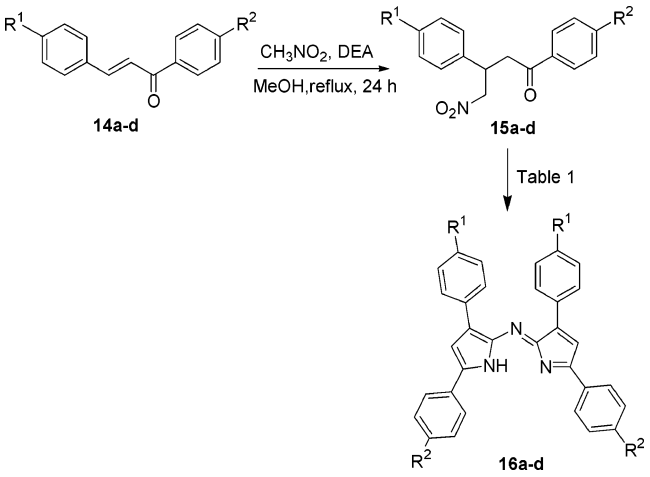

12 into a more structurally constrained architecture if they were to be exploited for the development of PDT agents. This we proposed could be achieved by conversion into their corresponding BF_2 chelates **13**, which would prevent the isomerization around the pyrrole carbon to bridging nitrogen bonds.[23]

We now report the synthesis, photophysical properties, test for singlet oxygen production, cellular localization, and in vitro light-induced cytotoxicity assays for this new class of PDT agent. The majority of PDT agents investigated to date are based on polypyrrole macrocycles from which it can be synthetically difficult to generate an array of sequentially modified derivatives. However, our proposed class of non-porphyrin sensitizers would be a good starting point, as they are amenable to modification around the periphery of the sensitizer, which could allow for optimization of aspects of their photophysical and therapeutic properties. This sensitizer class differs from previously investigated non-porphyrin-related photosensitizers, as they are overall charge neutral compounds.

Results and Discussion

Synthesis and Purification. The starting point of our synthesis was the diaryl α,β-unsaturated ketones (chalcones) **14a**−**d** of which many are commercially available or are readily made by an aldol/dehydration reaction of the corresponding aldehyde and acetophenone (Scheme 1).[24] The Michael addition of nitromethane to the α,β-unsaturated ketones, with diethylamine (DEA) as base, yields the 1,3-diaryl-4-nitrobutan-1-ones, **15a**−**d** in high yields. These two classical organic synthesis reactions provide the precursors to the tetraarylazadipyrromethenes very efficiently.

Our initial approach for the generation of tetraarylazadipyrromethenes **16a**−**d** was based on the method first reported by Rogers but following this we undertook a detailed study of the reaction to refine the methodology.[22] The previously reported synthesis of tetraphenylazadipyrromethene **16a** used a solventless reaction at 180 °C between **15a** and an excess of ammonium formate (Scheme 1). We repeated these conditions as described and for **16a** achieved a comparable yield of 34% to that first reported (Table 1, entry 1). We tested ammonium acetate as an alternative ammonium source for the synthesis of **16a** and discovered the reaction to be successful with an improved isolated yield of 47% (entry 2). The same trend of improved yields was also observed for **16b** when substituting ammonium acetate for ammonium formate under solventless conditions (entries 6 and 7).

Table 1. Reaction Optimization for **16a**−**d**

entry	compd	R^1	R^2	reagent/solvent	time/h	% yield[a]
1	**16a**	H	H	NH_4CO_2H/none	1	34
2	**16a**	H	H	NH_4OAc/none	1.5	47
3	**16a**	H	H	NH_4CO_2H/EtOH	24	33
4	**16a**	H	H	NH_4OAc/EtOH	24 (48)	35 (42)
5	**16a**	H	H	NH_4OAc/BuOH	24	39
6	**16b**	H	OCH_3	NH_4CO_2H/none	1.5	33
7	**16b**	H	OCH_3	NH_4OAc/none	1.5	45
8	**16b**	H	OCH_3	NH_4OAc/EtOH	24	24
9	**16b**	H	OCH_3	NH_4OAc/BuOH	24	47
10	**16c**	OCH_3	H	NH_4OAc/none	0.5	46
11	**16c**	OCH_3	H	NH_4OAc/EtOH	48	23
12	**16c**	OCH_3	H	NH_4OAc/BuOH	48	48
13	**16d**	Br	H	NH_4OAc/none	1.5	15
14	**16d**	Br	H	NH_4OAc/EtOH	24 (48)	16 (22)
15	**16d**	Br	H	NH_4OAc/BuOH	24	24

[a] Isolated purified yield.

To replace the harsh solventless methodology and develop a more synthesis-friendly reaction procedure, we investigated the reaction in various solvents. Encouragingly, we found that the reaction could be readily achieved by heating under reflux in either ethanol or butanol for time periods of 24−48 h. The reaction of **15a** with ammonium acetate in ethanol under reflux for 24 h gave a 35% isolated yield of **16a**. This yield could be increased to 42% by lengthening the reaction time to 48 h (Table 1, entry 4). Substituting butanol for ethanol as reaction solvent gave an improved yield of **16a** of 39% over a 24 h reaction period (entry 5). A similar trend was observed for **16b**−**d** in that higher isolated yields were obtained in butanol than ethanol (entries 9, 12, and 15). In general, the reaction gave higher yield in butanol or the solventless conditions in comparison to ethanol.

As each method gave the desired product, some of the advantages or drawbacks of each procedure are associated with product purification. The solventless reactions require the harshest conditions, but have an advantage of the shortest reaction time. Upon completion of these reactions the product is a solid mass in the reaction flask and requires silica gel chromatography for purification. When ethanol or butanol was used as the solvent, the product precipitated during the reaction and could be isolated by simple filtration in each case. The overall facile synthesis and purification of the tetraarylazadipyrromethenes **16** makes this class of chromophore very attractive as a starting point for the development of an array of novel PDT therapeutics.

We next sought an efficient synthetic method to introduce a heavy atom onto **16** and chose to exploit the high reactivity of the pyrrole ring to electrophilic aromatic substitution to accomplish this. Bromination of both the unsubstituted β-pyrrole positions of **16a**−**c** was readily achieved by their reaction with bromine at room temperature, yielding **17a**−**c** in excellent yields (Scheme 2). Conversion of **16a**−**d** and **17a**−**c** into their corresponding BF_2 chelates **18a**−**d** and **19a**−**c** was achieved by stirring with BF_3.etherate using diisopropylethylamine (DIEA) as base in dichloromethane at room temperature for 24 h, giving isolated purified yields ranging from 62 to 90% (Scheme 2). Purification of products was carried out by column

(23) (a) Killoran, J.; Allen, L.; Gallagher, J. F.; Gallagher, W. M.; O'Shea, D. F. *Chem. Commun*. **2002**, 1862. (b) O'Shea D.; Killoran J.; Gallagher, W. PCT, WO 03/080627 A1.
(24) Wattanasin, S.; Murphy, W. S. *Synthesis* **1980**, 647.

Scheme 2

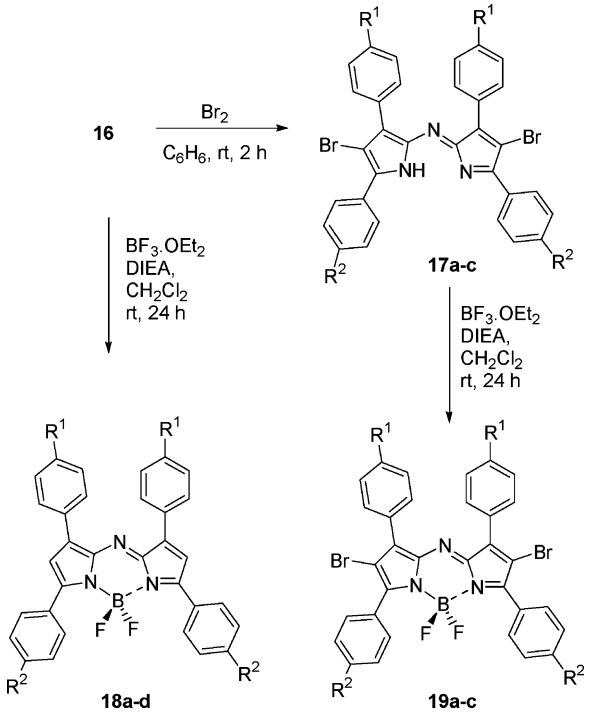

chromatography on silica gel prior to spectroscopic measurement and assaying.

An inherent advantage of our photosensitizer system is that the synthesis utilizes classical high-yielding organic synthetic reactions to generate their precursors, which can be easily transformed into the tetraarylazadipyrromethenes **16** in one facile step. Synthetic manipulation of **16** to facilitate the inclusion of the heavy-atom bromine is readily achievable, and conversion into their final chelates is routine. The compounds are polar but nonionic and are soluble in organic solvents such as THF, dichloromethane, or toluene.

Photosensitizer Formulation. To obtain aqueous solutions of **18a**−**d** and **19a**−**c** for spectroscopic analysis and in vitro assays, the emulsifier Cremophor EL (CrEL) was used. CrEL is a nonionic surfactant, frequently used in vivo as a delivery agent for poorly water soluble anticancer drugs such as Paclitaxel (taxol).[25] The formulation procedure required dissolving the photosensitizer in the minimum quantity of THF and treating the solution with a mixture of CrEL and 1,2-propanediol (10:3 v/v). This was sonicated for 1 h followed by removal of the THF under vacuum. The resulting blue/green oil was dissolved in phosphate-buffered saline (PBS) solution followed by filtration through a 0.2 μm membrane filter. To ensure the accuracy of the concentration, which may vary due to partial precipitation of the photosensitizer, the exact concentration was confirmed by UV−visible spectral analysis of the solutions prior to assaying.

Photosensitizer Spectroscopic Properties. The absorption spectra of **18a**−**d** and **19a**−**c** in aqueous formulated solution all show a strong $S_0 \rightarrow S_1$ transition with wavelength of maximum absorbance varying between 651 and 696 nm, depending upon substituents (Figure 5, Table 2). We have observed a striking dependence of absorption maxima on

(25) Gelderblom, H.; Verweij, J.; Nooter, K.; Sparreboom, A. *Eur. J. Cancer* **2001**, *37*, 1590.

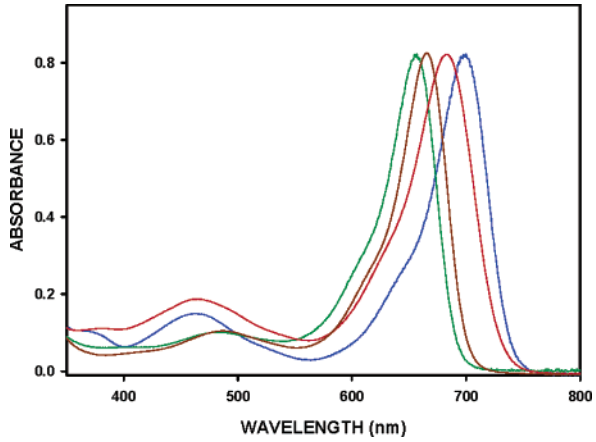

Figure 5. UV−visible spectra of **18a** (green), **18b** (blue), **18d** (brown), and **19b** (red) in H_2O/CrEL.

Table 2. Spectroscopic Absorbance Properties of **18a**−**d** and **19a**−**c**[a]

		λ_{max}/nm				fwhm/nm		
entry	compd	H_2O/CrEL	toluene	ethanol	chloroform	H_2O/CrEL	chloroform	ϵ[b]/M^{-1} cm^{-1}
1	**18a**	658	655	647	650	53	49	79 000
2	**18b**	696	693	686	688	57	55	85 000
3	**18c**	671	666	660	664	57	57	78 000
4	**18d**	666	662	655	658	51	47	83 000
5	**19a**	651	652	645	650	57	47	79 000
6	**19b**	683	683	675	679	67	57	75 000
7	**19c**	655	655	646	653	66	57	80 000

[a] Concentration 5×10^{-6} M, rt. [b] Chloroform.

substituents on the aryl rings. An aqueous solution of the tetraphenyl-substituted "parent" molecule **18a** has a λ_{max} within the therapeutic window spectral region at 658 nm (Figure 5, Table 2). Introduction of an electron-donating methoxy group onto the para position of the aryl rings α to the pyrrole nitrogen in **18b** ($R^2 = OCH_3$) results in a significant bathochromic shift of 38 nm (Figure 5, Table 2, entry 2). Interestingly, para-substitution with a methoxy moiety on both of the aryl rings in the β-pyrrole positions of **18c** ($R^1 = OCH_3$) had significantly less impact, with a bathochromic shift of 13 nm (Table 2, entry 3). In comparison, **18d**, which contains an electron-withdrawing group (R^1 = Br) in the same position, resulted in a minor bathochromic shift of 8 nm.

Comparisons of **18a**−**c** with their corresponding dibrominated derivatives **19a**−**c** show that introduction of the heavy atoms gives rise to a moderate hypsochromic shift, ranging from 7 to 16 nm. Remarkably, the substitution of bromines onto the pyrrole rings results in only minor changes in the maxima or the shape of the absorption bands. For example, a comparison of **18a** and **19a** in aqueous solution show only a variance of 7 nm in their λ_{max} values (Table 2, entries 1 and 5). This demonstrates that the heavy atom can be introduced without diminishing the advantageous absorption characteristics of our photosensitizers. In general, the absorbance characteristics of this class of photosensitizer are relatively insensitive to solvent effects with small hypsochromic shifts (6−9 nm) observed in the polar solvent ethanol when compared to a nonpolar solvent such as toluene (Table 2). The spectral bandwidth of the principal absorption band can be analyzed by the full width at half-maximum (fwhm) values, which vary from 51 to 67 nm in aqueous solutions. This sharp absorption band is indicative of

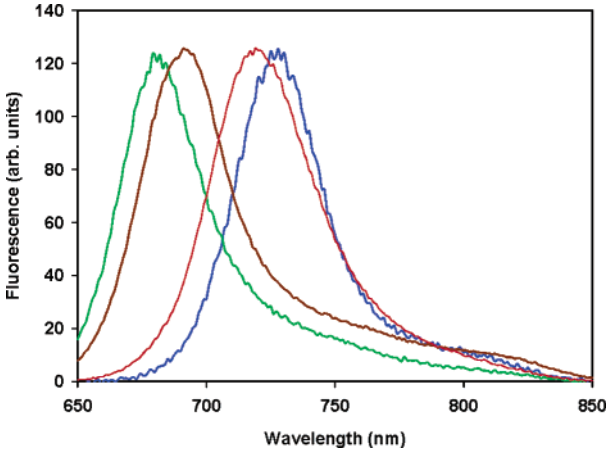

Figure 6. Fluorescence spectra of **18a** (green), **18b** (blue), **18d** (brown), and **19b** (red) in H_2O/CrEL.

Table 3. Spectroscopic Fluorescence Properties of **18a**−**d** and **19a**−**c**[a]

			λ_{max}[b]/nm				
entry	compd	Stoke shift[b]/nm	H_2O/CrEL	toluene	ethanol	chloroform	Φ_f[c]
1	**18a**	25	683	676	669	672	0.34
2	**18b**	31	727	717	715	715	0.36
3	**18c**	30	701	693	697	695	0.23
4	**18d**	22	688	683	677	680	0.34
5	**19a**	28	679	672	666	673	0.01
6	**19b**	36	719	714	712	714	0.1
7	**19c**	38	693	683	680	679	<0.01

[a] Concentration 2×10^{-7} M, rt. [b] H_2O/CrEL. [c] Chloroform.

a nonaggregated system in these solutions, as the observed values are comparable to those in chloroform, which vary from 47 to 57 nm (Table 2).

The extinction coefficients of this class of photosensitizer are in the range of 75 000−85 000 M^{-1} cm^{-1}, which is a significant improvement over substituted porphyrins (3000−5000) or chlorins (30 000−40 000) and is only matched in this region of the absorption spectrum by phthalocyanine or cyanine dyes (150 000−250 000).[1c] This relatively high extinction coefficient within the therapeutic window is an advantage over other PDT agents such as Photofrin or protoporphyrin IX **2**, as the most efficiently excited photosensitizers are those that have strong absorption bands in this region of the spectrum. This strong absorbance is one of the factors that can facilitate a high singlet-oxygen generation when using therapeutic irradiance conditions of wavelengths greater than 650 nm. Conversely, it is also of some advantage that the extinction coefficient is not too high, as this can limit light penetration in vivo due to the self-shielding effect of a sensitizer.[26]

The fluorescence properties of the sensitizers were examined in aqueous formulated solutions, toluene, ethanol, and chloroform. Excitation of the compounds **18a**−**d** and **19a**−**c** in aqueous solutions at 630 nm all gave fluorescence bands that were mirror images of the absorbance spectra with Stoke shifts in the range of 22−38 nm (Figure 6, Table 3). Overall, the emission spectra were relatively insensitive to solvent effects, with small hypsochromic shifts observed in ethanol when compared to toluene. For example, wavelength maximum of emission for **18a** is 676 nm in toluene and 669 nm in ethanol (Table 3, entry 1). The compounds **18a**−**d** showed a range of high fluorescence quantum yields (Φ_f) measured in chloroform from 0.23 to 0.36 (Table 3). Interestingly, the quantum yield for the bromoaryl-substituted derivative **18d** did not show a significant decrease in fluorescence quantum yield when compared to **18a**, but as the bromine substituents are distant from the central core of the photosensitizer, it could be anticipated that a significant heavy-atom effect may not be observed. In comparison, the introduction of bromine directly into the core of the photosensitizer gave rise in each case to substantial reduction in fluorescence quantum yields for **19a**−**c** (Table 3, entries 5−7). This would indicate that when bromine is directly substituted onto the central core of the photosensitizer, a larger heavy-atom effect can be induced that, depending upon other possible competing photophysical pathways, may translate into increased singlet oxygen production.

Heavy-Atom Effect and Singlet-Oxygen Generation. An electronic transition from a singlet to a triplet excited state within a molecule is a spin-forbidden process and as such occurs inefficiently for many compounds. In order for a transition between states of different spin multiplicities to occur effectively, a spin−orbit perturbation is generally required.[27] Enhanced spin−orbit perturbations can be achieved by the attachment of a heavy atom directly onto the molecule[28] (internal heavy-atom effect) or placing the molecule in a surrounding environment containing heavy atoms[29] (external heavy-atom effect). We chose to exploit the internal heavy-atom approach, but in an attempt to effect varying degrees of spin−orbit coupling, we placed the heavy atoms at two different positions in the molecule. This we anticipated would allow us to modulate the degree of spin−orbit coupling and hence the efficiency of singlet oxygen production by three modes: (i) no heavy atom within the sensitizer, thereby relying on the inherent spin−orbit coupling of the molecule; (ii) positioning of bromines on the aryl rings (not directly on the sensitizer), which could give rise to an intermediate singlet-oxygen generation level (termed an intramolecular external heavy-atom effect);[30] and (iii) positioning of the bromine directly onto the sensitizer, thereby fully exploiting the internal heavy-atom effect and providing the most efficient singlet-oxygen producers (Figure 7).[31]

The final step of the singlet-oxygen generation process is an energy transfer from photosensitizer triplet state to ground-state oxygen. An additional consequence of introducing heavy-atom substituents can be to give rise to nonradiative internal back-conversion to the ground state or inhibiting the photosensitizer triplet to ground-state oxygen energy transfer. These competing pathways would give rise to loss of the excited-state energy without the generation of singlet oxygen. This makes the position of the heavy-atom within the sensitizer critical, as the atom(s) must be positioned to have a substantial effect on the degree of spin−orbit coupling but not give rise to competing excited-state energy loss pathways. As such a heavy atom can

(26) Dougherty, T. J.; Potter, W. R. *J. Photochem. Photobiol. B* **1991**, *8*, 233.
(27) Lower, S. K.; El-Sayed, M. A. *Chem. Rev.* **1966**, *66*, 199.
(28) (a) Yuster, P.; Weissman, S. I. *J. Chem. Phys.* **1949**, *17*, 1182. (b) McClure, D. S. *J. Chem. Phys.* **1949**, *17*, 905.
(29) (a) Koziar, J. C.; Cowan, D. O. *Acc. Chem. Res.* **1978**, 334 (review). (b) McGlynn, S. P.; Reynolds, M. J.; Daigre, G. W.; Christodoyleas, N. D. *J. Phys. Chem.* **1962**, *66*, 2499. (c) Kasha, M. *J. Chem. Phys.* **1952**, *20*, 71.
(30) Chandra, A. K.; Turro, N. J.; Lyons, A. L., Jr.; Stone, P. *J. Am. Chem. Soc.* **1978**, *100*, 4964.
(31) For this description, we regard the fused five−six−five-membered rings as the central sensitizer and the aryl rings as peripheral substituents.

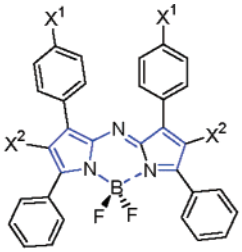

(i) X^1, X^2 = H: inherent spin-orbit coupling
(ii) X^1 = Br, X^2 = H: intramolecular external heavy atom effect
(iii) X^1 = H, X^2 = Br: internal heavy atom effect

Figure 7. Positioning of the bromine heavy atoms around the core sensitizer (blue).

promote an $S_1 \rightarrow T_1$ ISC, though it may not necessarily result in enhanced singlet-oxygen production. This effect has been reported for the pyrylium class of PDT agents **11**, which following the replacement of the ring oxygen with the heavier atom tellurium did not give rise to an increase in singlet-oxygen quantum yields, even though a significant decrease in the fluorescence quantum yields was observed (Figure 2).[18b] Similarly, substitution of two pyrrole nitrogen atoms of *meso*-tetraarylporphyrins for selenium atoms also gave reduced singlet-oxygen quantum yields when compared to the parent porphyrin.[32] In both cases this has been explained by the fact that the larger atomic radii of the heavy atoms led to structural distortions of the pyrylium and porphyrin rings, giving rise to loss of sensitizer planarity, which promoted nonradiative decay to the ground state and as a result a decrease in singlet-oxygen quantum yields. This effect may also be attributed to a shortening of the triplet lifetime as a result of the internal heavy-atom effect.[21,29a] Recently polyhalogenated *meso*-tetraarylporphyrins and bacteriochlorins have been shown to modulate their singlet-oxygen quantum yields in organic solutions, depending upon the position and number of halo substituents.[33]

X-ray Structure of 19a. As the introduction of a heavy atoms with large atomic radii into a photosensitizer can result in structural deformation to the planarity of the molecule, we sought to gain structural evidence for the effects, if any, on our sensitizer structure imparted by the bromine atoms in **19a**−**c**. **19a** crystallized, by the slow room-temperature evaporation of a toluene solution, in the monoclinic space group *Cc* (#9) with four molecules in the unit cell. A thermal ellipsoid drawing of **19a** is shown in Figure 8.

The molecular structure confirmed the conjugated nature of this class of sensitizer with comparable bond lengths for the bridging nitrogen (N3) to both pyrrole rings (C1, C17) and for the pyrrole nitrogen (N1, N2) to boron bond lengths. A comparison of all bond lengths of both pyrrole rings of **19a** showed them to be equivalent (Table 4).

Despite the introduction of two bromine atoms onto the sensitizer **19a**, the planarity of the central 12-atom core of the

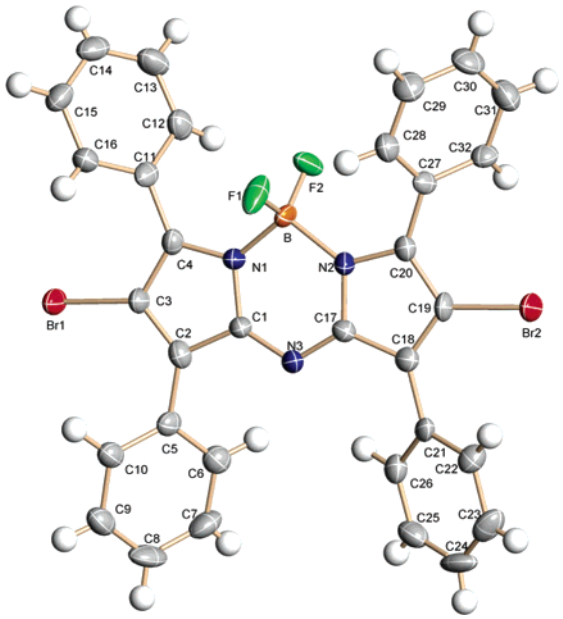

Figure 8. Perspective drawing of **19a.** Thermal ellipsoids drawn at the 80% probability level.

Table 4. Selected Bond Lengths for **19a**

bond	length/Å	bond	length/Å
C(1)−N(3)	1.322(3)	C(17)−N(3)	1.322(3)
C(1)−N(1)	1.395(3)	C(17)−N(2)	1.393(3)
C(1)−C(2)	1.439(3)	C(17)−C(18)	1.443(4)
C(2)−C(3)	1.375(4)	C(18)−C(19)	1.382(4)
C(3)−C(4)	1.429(4)	C(19)−C(20)	1.421(4)
C(3)−Br(1)	1.880(2)	C(19)−Br(2)	1.870(2)
C(4)−N(1)	1.355(3)	C(20)−N(2)	1.359(3)
N(1)−B	1.568(4)	N(2)−B	1.564(3)
B−F(1)	1.372(4)	B−F(2)	1.379(3)

molecule was preserved. The bromine bond angles from pyrrole ring 1 (N1/C1/C2/C3/C4) are −0.126(1) Å for Br(1) and 0.109(1) Å for Br(2) from planarity and for pyrrole ring 2 (N2/C17/C18/C19/C20) Br(1) is −0.415(1) Å and Br(2) is 0.004 Å. The angle of intersection of pyrrole ring 1 and pyrrole ring 2 is small at 4.2(2)°. The 12-atom plane of the central tricyclic structure shows the greatest deviation from this plane of 0.100(2) Å for the atom N(1). This compares favorably with our previously reported structure of nonbrominated **18b**, which has a comparable intersect angle of pyrrole ring 1 and pyrrole ring 2 of 4.1(3)°.[23a] Additionally, the central tricyclic 12-atom plane of **18b** shows the greatest deviation from this plane of 0.087(3) Å for the atom N(2). This lends weight to the supposition that introduction of the bromines at the β-pyrrole position of **19a**−**c** could give rise to a more efficient population of the triplet state without causing an increase in nonradiative decay to the ground state.

Comparative Study of Singlet-Oxygen Generation in Solution with Light > 600 nm. To test our ability to gain control over singlet-oxygen production by exploiting the heavy-atom effect, we carried out a comparative singlet-oxygen generation analysis. The study was undertaken by monitoring the reaction of the known singlet oxygen acceptor 1,3-diphenylisobenzofuran (DPBF) with photosensitizer-generated singlet oxygen.[34] This was achieved experimentally by following the disappearance of the 410 nm absorbance band of DPBF at

(32) (a) You, Y.; Gibson, S. L.; Hilf, R.; Davies, S. R.; Oseroff, A. R.; Roy, I.; Ohulchanskyy, T. Y.; Bergey, E. J.; Detty, M. R. *J. Med. Chem.* **2003**, *46*, 3743. (b) Hilmey, D. G.; Abe, M.; Nelen, M. I.; Stilts, C. E.; Baker, G. A.; Baker, S. N.; Bright, F. V.; Davies, S. R.; Gollnick, S. O.; Oseroff, A. R.; Gibson, S. L.; Hilf, R.; Detty, M. R. *J. Med. Chem.* **2002**, *45*, 449.

(33) (a) Pineiro, M.; Rocha Gonsalves, A. M. d'A.; Pereira, M. M.; Formosinho, S. J.; Arnaut, L. G. *J Phy. Chem. A* **2002**, *106*, 3787. (b) Azenha, E. G.; Serra, A. C.; Pineiro, M.; Pereira, M. M.; de Melo, J. S.; Arnaut, L. G.; Formosinho, S. J.; Rocha Gonsalves, A. M. d'A. *Chem. Phy.* **2002**, *280*, 177.

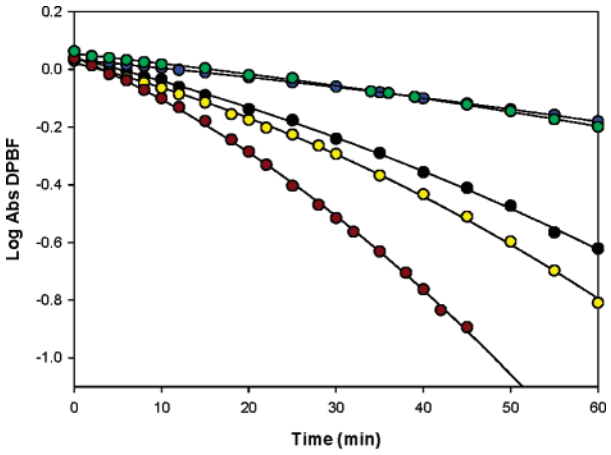

compound	1	18a	18b	18c	18d
rel. rate	1	0.46	0.4	1.2	1.7

Figure 9. Comparative singlet-oxygen generation of **18a** (green), **18b** (blue), **18c** (yellow), **18d** (brown), and hematoporphyrin **1** (black) at 5×10^{-6} M concentration.

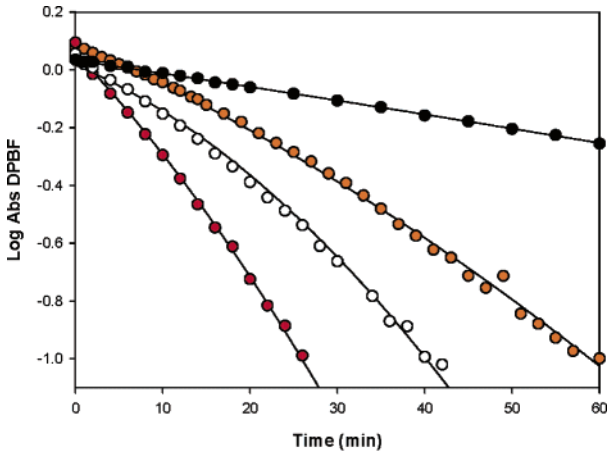

compound	9	19a	19b	19c
rel. rate	1	2.9	7.7	4.2

Figure 10. Comparative singlet-oxygen generation of **19a** (orange), **19b** (red), **19c** (white), and methylene blue **9** (black) at 5×10^{-8} M concentration.

initial concentration of 5×10^{-5} M over a time period of 1 h. We used a filtered light source of wavelength > 600 nm, which would mimic those used for our in vitro assays or those used in a clinical therapeutic setting. Each of the sensitizers **18a**−**d** was examined at a concentration of 5×10^{-6} M and compared to hematoporphyrin **1** as a reference sensitizer. The brominated pyrrole derivatives **19a**−**c** were examined at a lower concentration of 5×10^{-8} M and compared to the reference sensitizer methylene blue **9**. Relative rates of oxygenation of DPBF by **18a**−**d** and **19a**−**c** versus the standards **1** and **9** were estimated by comparison of the rates of consumption of DPBF at the initial stages of each experiment.[35] The standard sensitizers **1** and **9** both have high singlet-oxygen quantum yields of 0.65 and 0.50, respectively, in methanol, though these values are not necessarily an accurate indicator for the efficiency of singlet-oxygen generation under therapeutic irradiance conditions, as the extinction coefficient of the sensitizer at the irradiation wavelengths (above 600 nm) is also a key contributing factor.[36,18a] The experimental results showed that **18a** and **18b** had moderate singlet-oxygen production over the 1 h time period, whereas **18c** gave a better production of singlet oxygen comparable to that of reference **1** (Figure 9). This confirmed that our new class of photosensitizer has some inherent spin−orbit coupling. **18d**, which has two bromo-substituted aryl rings, did show an enhanced singlet-oxygen generation over the other derivatives **18a**−**c** and **1**, as would be expected if the intramolecular external heavy-atom effect contributed to spin−orbit coupling. These results prove that we have achieved a range of varying singlet-oxygen generation profiles at a single photosensitizer concentration with a greater than 4-fold rate distribution from least effective **18b** to most active **18d** (Figure 9).

It would be anticipated that to achieve the greatest internal heavy-atom effect the bromines should be incorporated directly on the central core of the photosensitizer. This was borne out for **19a**−**c**, which all showed an increased efficiency of singlet-oxygen generation in comparison to **18a**−**c**, even at a 100-fold lower concentration of 5×10^{-8} M (Figure 10). Each of our tested photosensitizers performed better than **9**, with **19b** being the best, having a 7.7-fold rate enhancement when compared to the reference (Figure 10). This is evidence that the heavy-atom effect can be exploited to deliver controlled levels of the key cytotoxic agent for our photosensitizer class. The dramatically enhanced singlet-oxygen production levels of **19a**−**c**, when contrasted with **18a**−**c**, show that the inclusion of the heavy atom as a substituent directly onto the central core of the photosensitizer has achieved our desired aim and has not given rise to loss of excited-state energy by internal radiationless transitions. No significant photobleaching of the sensitizers was observed during these experiments (see the Supporting Information).

As the incorporation of the bromine substituents can be achieved by one facile high-yielding synthetic transformation, this approach lends itself to tailoring a singlet-oxygen quantum yield of photosensitizer to the specific therapeutic requirements that are being addressed.

Photosensitizer Cellular Localization. To ascertain the cellular localization of our photosensitizers, we chose **18a** as a representative compound, due to its inherent high fluorescence quantum yield, which would enable facile visualization with fluorescence microscopy. Incubation of HeLa cervical carcinoma cells with 1×10^{-5} M aqueous **18a** (CrEL formulated) for 1 h at 37 °C gave rise to an efficient cellular uptake of photosensitizer as determined by fluorescence microscopy (Figure 11). The imaged cells displayed an uptake of **18a** that appeared to be localized to the cytoplasm (red color), with the nuclei remaining free of photosensitizer (dark area).

To confirm cytoplasmic localization of our photosensitizers, a confocal laser scanning microscopy (CLSM) study was carried out. CLSM allows for the 3-D imaging of fluorescent compounds within a single cell.[37] The 3-D reconstruction of the cellular distribution of **18a** in HeLa cells was determined by the combination of 20 focal plane sections of 0.5−1 μm apart through a single cell. CLSM confirmed that the subcellular

(34) Gollnick, K.; Griesbeck, A. *Tetrahedron* **1985**, *41*, 2057.
(35) Kochevar, I. E.; Redmond, R. W. *Methods Enzymol.* **2000**, *319*, 20.
(36) Reddi, E.; Rodgers, M. A. J.; Spikes, J. D.; Jori, G. *Photochem. Photobiol.* **1984**, *40*, 415.
(37) Shotton, D. M. *J. Cell Sci.* **1989**, *94*, 175.

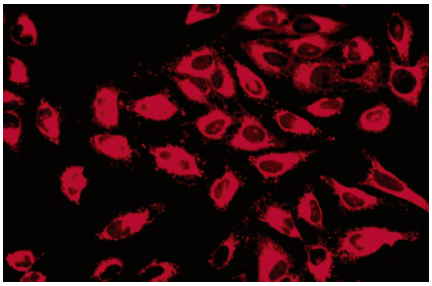

Figure 11. Fluorescence microscope (rhodamine filter) imaging of HeLa cervical carcinoma cells following incubation with **18a** (red color); dark areas are the cell nuclei.

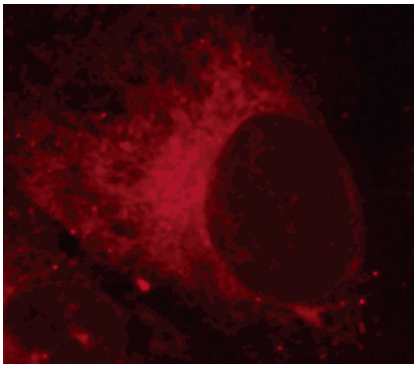

Figure 12. CLSM image of a HeLa cell following incubation with **18a** (red color); the dark area is the cell nucleus (see the Supporting Information).

localization of **18a** was exclusive to the cytoplasm with no nuclear localization detected (Figure 12) (see the Supporting Information).

To prove the perinuclear localization of our photosensitizers, a dual staining experiment was carried out. HeLa cells were incubated for 1 h with **18a**, followed by the treatment of the cells with the green nucleic acid stain SYTOX green.[38] **18a** and SYTOX green were excited with a 1 mW green helium neon (HeNe) 543 nm laser and a 50 mW argon 488 nm laser, respectively. Simultaneous detection of cell-bound **18a** and the nuclear probe SYTOX green was achieved using 640−730 and 505−550 nm band-pass filters, respectively. The results gave excellent contrast imaging between the green nuclear region and the red cytoplasm, proving that **18a** localizes to areas of the cell other than the nucleus (Figure 13) (see the Supporting Information). The absence of nuclear localization suggests that this class of compound would not induce direct nuclear DNA damage but mediate their actions at extranuclear targets. This selective localization to the cytoplasm could be attributed to some extent to the fact that these compounds are charge neutral.

Light-Induced Cytotoxicity Assay. Two different cell types were examined in the assay, MRC5-SV40 transformed fibroblast cells and HeLa cells. Varying concentrations of CrEL formulated[39] aqueous solutions of the photosensitizers **18a**, **18b**, **18d**, and **19b** were incubated with the cells in the dark for 3 h. Subsequently, the culture medium was removed and fresh culture medium added to each well. The plates were irradiated using a light source of wavelength 600−750 nm delivering a

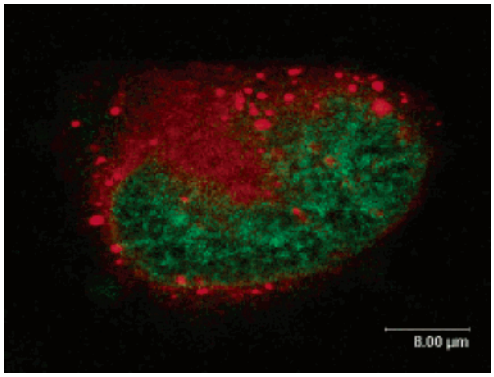

Figure 13. CLSM image of a HeLa cell following incubation with **18a** (red color) and nuclear stain SYTOX green (green color) (see the Supporting Information).

light dose of either 8 or 16 J cm^{-2}.[40] Following irradiation, the cells were incubated for a further 48 h at 37 °C, after which time the percentage cell viability was determined using a tetrazolium chlorimetric reduction assay. Dark toxicity of photosensitizers was determined by carrying out an identical experiment as described above except that the light irradiation step was omitted (0 J cm^{-2}). All assay experiments were carried out in triplicate and an average of the three individual runs are presented. Hematoporphyrin **1** was used as a comparative standard control and was assayed according to previously documented procedures.[41]

In our assay system, MRC5-SV40 cells displayed no determinable dark toxicity with **18a**, **18b**, **19b**, or **1** up to a concentration of 10^{-4} M, whereas for **18d**, dark toxicity was observed at high concentrations with a calculated EC_{50} value of 7.1×10^{-4} M (Figure 14a, Table 5). In contrast, irradiation with 8 J cm^{-2} light dose showed a significant light-induced toxicity with EC_{50} values determined for **18a**, **18b**, and **19b** as 3.1×10^{-6}, 1.1×10^{-4}, and 3.7×10^{-8} M, respectively (Table 5). The exceptional light-induced toxicity of **19b** was very encouraging, as this molecule contained the two bromine heavy atoms directly substituted onto the core of the photosensitizer. Surprisingly **18d**, which has two bromine substituents on the benzene rings and was better that **18a**−**c** in the singlet-oxygen generation tests, performed poorly under these assay conditions, with an EC_{50} value of 2.3×10^{-4} M.

As phototoxicity should be dependent upon light dose as well as photosensitizer concentration, we repeated this assay series with a higher light irradiation of 16 J cm^{-2}. The higher light dose resulted in an improved EC_{50} value for each of our studied photosensitizers, with values obtained for **18a** at 5.0×10^{-7} M, **18b** at 1.7×10^{-5} M, **18d** at 2.8×10^{-4} M, and **19b** at 1.4×10^{-8} M (Figure 14b, Table 5). Each of our tested photosensitizers, apart from **18d**, performed better at this light dose than the standard control hematoporphyrin **1** (Table 5).

These data clearly portray how we have achieved a remarkable spectrum of activity (from the micro- to nanomolar range) across these structurally related sensitizers. In the case of **19b**, exploitation of the heavy-atom effect in vitro is seen to be a viable method to control the excited triplet-state population and

(38) Suzuki, T.; Matsuzaki, T.; Takata, K. *Acta Histochem. Cytochem.* **1998**, *31*, 297.
(39) No light or dark toxicity was observed for CrEL alone when tested in our assay system.
(40) The light source was either a Waldmann PDT 1200 L instrument with an emission spectrum of 600−750 nm or a 500 W halogen lamp combined with red and water filters with an emission spectrum of 600−750 nm. Both systems gave comparable assay data.
(41) Sol, V.; Blais, J. C.; Carré, V.; Granet, R.; Guilloton, M.; Spiro, M.; Krausz, P. *J. Org. Chem.* **1999**, *64*, 4431.

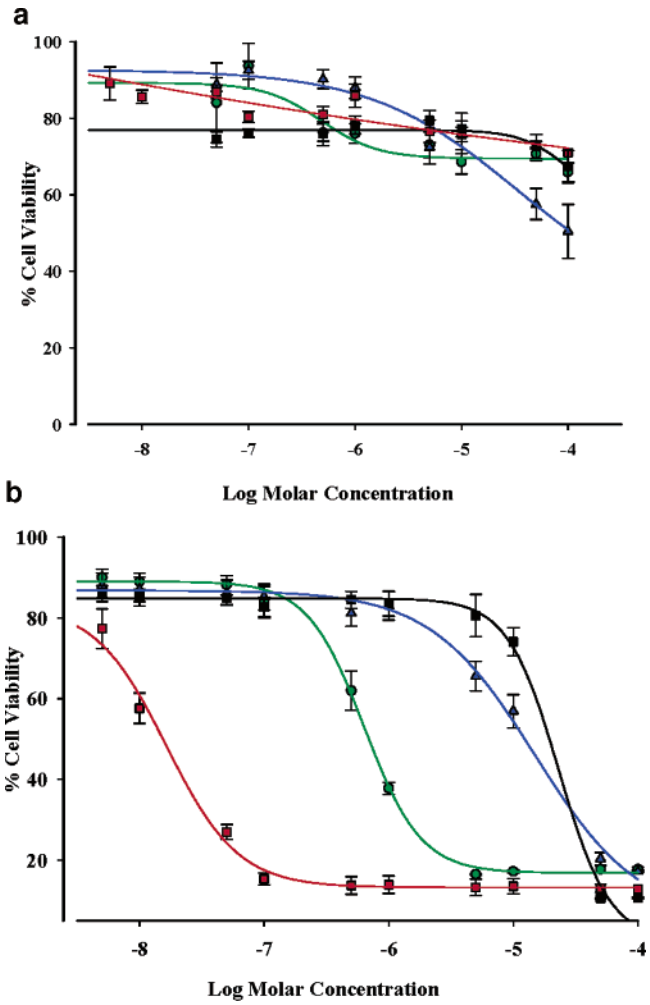

Figure 14. (a) Dark toxicity of **18a** (green), **18b** (blue), **19b** (red), and hematoporphyrin **1** for MRC5-SV40 cells. (b) Light-induced (16 J cm^{-2}) toxicity of **18a** (green), **18b** (blue), **19b** (red), and hematoporphyrin **1** (black) for MRC5-SV40 cells.

Table 5. In Vitro EC_{50} Assay Data for MRC5-SV40 Cells[a]

		EC_{50} (M)		
entry	compd	0 J cm^{-2}	8 J cm^{-2}	16 J cm^{-2}
1	**1**	ND	$(6.3 \pm 3) \times 10^{-5}$	$(3.7 \pm 1) \times 10^{-5}$
2	**18a**	ND	$(3.1 \pm 3) \times 10^{-6}$	$(5.0 \pm 1) \times 10^{-7}$
3	**18b**	ND	$(1.1 \pm 1) \times 10^{-4}$	$(1.7 \pm 1) \times 10^{-5}$
4	**18d**	$(7.1 \pm 2) \times 10^{-4}$	$(2.3 \pm 2) \times 10^{-4}$	$(2.8 \pm 2) \times 10^{-4}$
5	**19b**	ND	$(3.7 \pm 0.3) \times 10^{-8}$	$(1.4 \pm 0.1) \times 10^{-8}$

[a] Standard deviation in brackets.

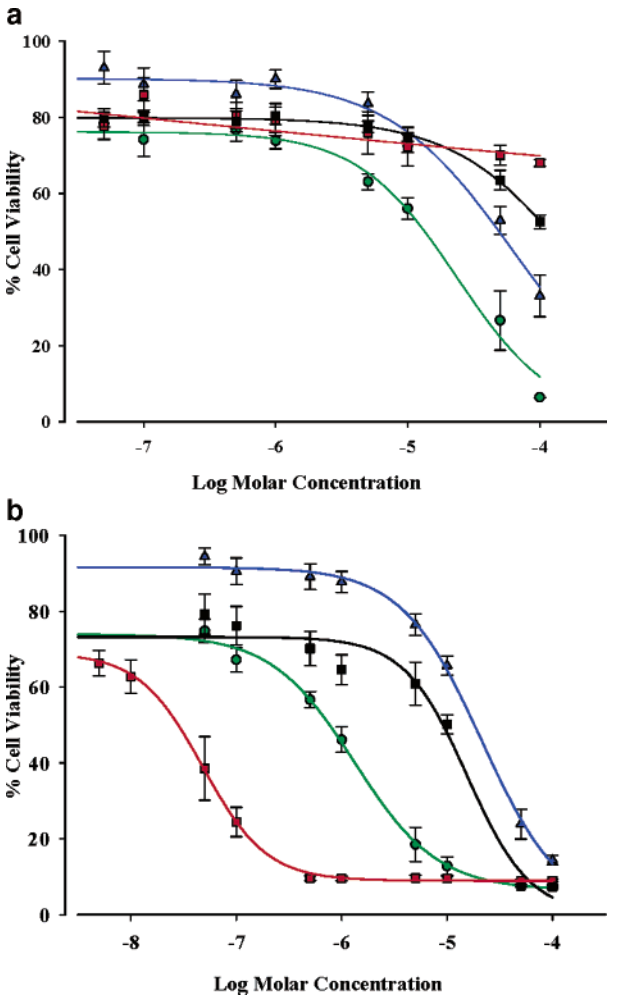

Figure 15. (a) Dark toxicity of **18a** (green), **18b** (blue), **19b** (red), and hematoporphyrin **1** (black) for HeLa cells. (b) Light-induced (16 J cm^{-2}) toxicity of **18a** (green), **18b** (blue), **19b** (red), and hematoporphyrin **1** (black) for He La cells.

Table 6. In Vitro EC_{50} Assay Data for HeLa Cells[a]

		EC_{50} (M)		
entry	compd	0 J cm^{-2}	8 J cm^{-2}	16 J cm^{-2}
1	**1**	ND	$(3.3 \pm 2) \times 10^{-5}$	$(1.9 \pm 0.4) \times 10^{-5}$
2	**18a**	$(2.7 \pm 1) \times 10^{-5}$	$(2.8 \pm 0.7) \times 10^{-6}$	$(9.2 \pm 1) \times 10^{-7}$
3	**18b**	$(1.1 \pm 1) \times 10^{-4}$	$(7.2 \pm 5) \times 10^{-5}$	$(3.1 \pm 1 \times 10^{-5}$
4	**18d**	$(6.7 \pm 2) \times 10^{-4}$	$(1.5 \pm 1) \times 10^{-4}$	$(3.4 \pm 1) \times 10^{-5}$
5	**19b**	ND	$(6.3 \pm 2) \times 10^{-8}$	$(4.1 \pm 3) \times 10^{-8}$

[a] Standard deviation in brackets.

singlet-oxygen quantum yields, as well as to translate that control into significantly greater in vitro efficacy. It should be noted that in structural terms **18b** and **19b** only differ by the two bromine substituents, which gives rise to a divergence in efficacy by over a 1000-fold.

A second identical study was carried out using the HeLa cell line. Photosensitizer dark toxicity was only observed at high concentrations for **18a**,**b**,**d**, with our most active compound **19b** showing no observable dark toxicity in the tested concentration range (Figure 15a, Table 6). A broad range of light-induced cytotoxicity was also observed for the photosensitizer series in HeLa cells that was comparable to that observed in the MRC5-SV40 cell line. The determined EC_{50} values for the series with a light dose of 16 J cm^{-2} showed that **18b** (3.1×10^{-5} M) was the least active in our assay, followed by significantly improved results for **18a** (9.2×10^{-7} M) and the best being **19b** (4.1×10^{-8} M) (Figure 15b, Table 6). In this series both **18b** and **18d** were marginally out-performed by the standard hematoporphyrin **1**. An improvement in efficacy for each photosensitizer was observed on increasing the light dose from 8 to 16 J cm^{-2}, again showing the expected light-dose response behavior. Again, the in vitro heavy-atom effect was clearly observed; when comparing EC_{50} data for **18b** and **19b** at a light dose of 8 J cm^{-2}, there was over a 1000-fold efficacy increase while at 16 J cm^{-2} there was greater than a 750-fold increase (Table 6).

An overview of the compounds studied shows that we can clearly control the degree of light induced cytotoxicity of our new PDT agent class by minor structural modifications about

the core of the sensitizer. The low activity of **18d** in both tested cell lines is a reminder of the difficulty of prediction of how a photosensitizer will perform in a cellular system, as for this case the promising singlet-oxygen production tests did not translate into improved efficacy. On the basis of the in vitro assay data, we conclude that for the photosensitizers **18a** and **19b**, there is a clear potential for their development into new PDT agents, whereas **18b** would have more practical applications in tumor imaging, due to its high fluorescence quantum yield and low light and dark toxicity.

Conclusions

We have described an optimized synthesis and the photophysical characteristics of a new class of photosensitizer that has a significant potential to deliver PDT agents that could be individually fine-tuned for an exact therapeutic requirement. Minor structural modification about the periphery of the core photosensitizer allows for control over key features such as absorption maximum and singlet-oxygen generation. These properties are translated into control over light-induced toxicity in vitro. We are currently developing new modifications that will facilitate tumor cell selectivity and specific subcellular localization of the PDT agents. On a wider basis, the phthalocyanine-like spectral properties of these compounds and their unchelated precursors, coupled with their ease of synthesis and structural manipulation, may elicit attention from researchers concerned with a wide range of applications, such as nonlinear optical media, chemical sensors, fluorescent biochemical assaying, optical storage media, and catalysis.

Experimental Section

(3,5-Diphenyl-1*H*-pyrrol-2-yl)(3,5-diphenylpyrrol-2-ylidene)amine (16a). Method A. A 50 mL round-bottomed flask was charged with **15a** (1.5 g, 5.57 mmol) and ammonium formate (12.3 g, 195 mmol) and set up to carry out a distillation. The reagents were heated with stirring on an isomantle at 180 °C until the distillation was complete (1−1.5 h). During the course of the reaction, the mixture turned an intense blue color, ammonia was evolved, and aqueous formic acid was distilled out of the reaction flask at 101−102 °C. The reaction mixture in the round-bottomed flask was allowed to cool to room temperature, dissolved in CH_2Cl_2 (200 mL), and washed with water (2 × 50 mL) and the organic layer dried over sodium sulfate. The reaction mixture was preabsorbed onto silica. The preabsorbed silica was placed on top of a bed of silica (150 g) in a sintered glass funnel and eluted with methanol. The silica was then eluted with CH_2Cl_2 to yield the product **16a** as a blue-black solid (0.43 g, 34%).

Method B. A 50 mL round-bottomed flask was charged with **15a** (2.5 g, 9.28 mmol) and ammonium acetate (25.05 g, 0.325 mol) and set up to carry out a distillation. The reagents were heated with stirring on an isomantle at 180 °C until the distillation was complete (1−1.5 h). During the course of the reaction, the mixture turned an intense blue color, ammonia was evolved, and liquid distilled out of the reaction flask over a temperature range of 125−140 °C. The reaction mixture in the round-bottomed flask was allowed to cool to room temperature, dissolved in CH_2Cl_2 (200 mL), and washed with water (2 × 50 mL) and the organic layer dried over sodium sulfate. The reaction mixture was preabsorbed onto silica. The preabsorbed silica was placed on top of a bed of silica (150 g) in a sintered glass funnel and eluted with methanol. The silica was then eluted with CH_2Cl_2 to yield the product **16a** as a blue-black solid (1.0 g, 47%).

Method C. A 100 mL round-bottomed flask was charged with **15a** (1.0 g, 3.71 mmol), ammonium formate (8.20 g, 0.13 mol), and ethanol (40 mL) and heated under reflux for 24 h. During the course of the reaction, the product precipitated from the reaction mixture. The reaction was cooled to room temperature and filtered and the isolated solid washed with ethanol (2 × 10 mL) to yield the product **16a** as a blue-black solid (0.28 g, 33%).

Method D. A 100 mL round-bottomed flask was charged with **15a** (1.0 g, 3.71 mmol), ammonium acetate (10.0 g, 0.13 mol), and ethanol (40 mL) and heated under reflux for 24 h. During the course of the reaction, the product precipitated from the reaction mixture. The reaction was cooled to room temperature and filtered and the isolated solid washed with ethanol (2 × 10 mL) to yield the product **16a** as a blue-black solid (0.30 g, 35%).

Method E. A 100 mL round-bottomed flask was charged with **15a** (1.0 g, 3.71 mmol), ammonium acetate (10.0 g, 0.13 mol), and butanol (40 mL) and heated under reflux for 24 h. The reaction was cooled to room temperature, the solvent concentrated to 10 mL and filtered, and the isolated solid washed with ethanol (2 × 10 mL) to yield the product **16a** as a blue-black solid (0.33 g, 39%), mp 287−289 °C. ^{1}H NMR ($CDCl_3$) δ: 8.04−8.08 (m, 4H), 7.94−7.97 (m, 4H), 7.33−7.57 (m, 12H), 7.21 (s, 2H) (NH not observed). ^{13}C NMR ($CDCl_3$) δ: 155.1, 149.6, 142.7, 133.7, 132.2, 130.1, 129.2, 129.1, 128.3, 128.0, 126.6, 114.9. IR (KBr disk) cm^{-1}: 1598. λ_{max} ($CHCl_3$) nm: 598. EI-MS: *m*/*z* 449. HRMS Calcd for $C_{32}H_{24}N_3$ $[M + H]^+$: 450.1970. Found: 450.1948. Anal. Calcd for $C_{32}H_{23}N_3$: C, 85.50; H, 5.16; N, 9.35. Found: C, 85.21; H, 5.12; N, 9.41.

[5-(4-Methoxyphenyl)-3-phenyl-1*H*-pyrrol-2-yl][5-(4-methoxyphenyl)-3-phenylpyrrol-2-ylidene]amine (16b). 15b (1.25 g, 4.17 mmol) and ammonium acetate (11.27 g, 0.146 mol) were dissolved in butanol (50 mL) and heated under reflux for 24 h. The reaction was cooled to room temperature, the solvent concentrated to 25 mL and filtered, and the isolated solid washed with ethanol (2 × 10 mL) to yield the product **16b** as a black-green solid (0.51 g, 47%), mp 238−240 °C. ^{1}H NMR ($CDCl_3$) δ: 8.04−8.07 (m, 4H), 7.90 (d, J = 8.8 Hz, 4H), 7.33−7.44 (m, 6H), 7.13 (s, 2H), 7.04 (d, J = 8.8 Hz, 4H), 3.91 (s, 6H) (NH not observed). ^{13}C NMR ($CDCl_3$) δ: 161.8, 154.2, 149.4, 142.4, 134.2, 129.2, 128.4, 128.3, 127.8, 125.5, 114.9, 114.7, 55.9. IR (KBr disk) cm^{-1}: 1600. λ_{max} ($CHCl_3$) nm: 621. EI-MS: *m*/*z* 509. HRMS Calcd for $C_{34}H_{28}N_3O_2$ $[M + H]^+$: 510.2182. Found: 510.2165. Anal. Calcd for $C_{34}H_{27}N_3O_2$: C, 80.13; H, 5.34; N, 8.25. Found: C, 79.89; H, 5.20; N, 8.28.

[3-(4-Methoxyphenyl)-5-phenyl-1*H*-pyrrol-2-yl][3-(4-methoxyphenyl)-5-phenylpyrrol-2-ylidene]amine (16c). 15c (1.0 g, 3.34 mmol) and ammonium acetate (9.0 g, 0.117 mol) were dissolved in butanol (50 mL) and heated under reflux for 24 h. The reaction was cooled to room temperature, the solvent concentrated to 25 mL and filtered, and the isolated solid washed with ethanol (2 × 10 mL) to yield the product **16c** as a brown solid (0.40 g, 48%), mp 290−292 °C. ^{1}H NMR ($CDCl_3$) δ: 8.03 (d, J = 8.6 Hz, 4H), 7.92−7.95 (m, 4H), 7.42−7.54 (m, 6H), 7.10 (s, 2H), 6.97 (d, J = 8.6 Hz, 4H), 3.88 (s, 6H) (NH not observed). ^{13}C NMR ($CDCl_3$) δ: 159.7, 155.0, 149.5, 142.3, 132.4, 130.4, 129.9, 129.1, 126.7, 126.5, 113.8, 113.6, 55.4. IR (KBr disk) cm^{-1}: 1605. λ_{max} ($CHCl_3$) nm: 608. EI-MS: *m*/*z* 509. HRMS Calcd for $C_{34}H_{28}N_3O_2$ $[M + H]^+$: 510.2182. Found: 510.2188. Anal. Calcd for $C_{34}H_{27}N_3O_2$: C, 80.13; H, 5.34; N, 8.25. Found: C, 79.98; H, 5.38; N, 7.99.

[3-(4-Bromophenyl)-5-phenyl-1*H*-pyrrol-2-yl][3-(4-bromophenyl)-5-phenylpyrrol-2-ylidene]amine (16d). 15d (0.3 g, 0.86 mmol) and ammonium acetate (2.3 g, 30.2 mmol) were dissolved in butanol (30 mL) and heated under reflux for 48 h. The reaction was cooled to room temperature, the solvent concentrated to 15 mL and filtered, and the isolated solid washed with ethanol (2 × 10 mL) to yield the product **16d** as a purple solid (0.062 g, 24%), mp 343−345 °C. ^{1}H NMR ($CDCl_3$) δ: 7.88−7.95 (m, 8H), 7.48−7.60 (m, 10H), 7.19 (s, 2H) (NH not observed). ^{13}C NMR ($CDCl_3$) δ: compound was too insoluble to record a spectrum. IR (KBr disk) cm^{-1}: 1542. λ_{max} ($CHCl_3$) nm: 603. EI-MS: *m*/*z* 607. HRMS Calcd for $C_{32}H_{22}Br_2N_3$ $[M + H]^+$: 606.0180. Found: 606.0192. Anal. Calcd for $C_{32}H_{21}Br_2N_3$: C, 63.28; H, 3.49; N, 6.92. Found: C, 62.96; H, 3.34; N, 6.69.

(4-Bromo-3,5-diphenyl-1*H*-pyrrol-2-yl)(4-bromo-3,5-diphenylpyrrol-2-ylidene)amine (17a). 16a (0.2 g, 0.44 mmol) was dissolved in dry benzene (20 mL) and treated with bromine (0.67 mL, 1.34 mmol) and the reaction stirred at room temperature for 2 h. The solvent was evaporated to dryness, yielding a black-green solid **17a** as the hydrobromide salt (0.3 g, 97%), mp 320−322 °C. ^{1}H NMR ($CDCl_3$) δ: 13.70 (bs, 2H), 8.21 (bs, 4H), 7.57−7.59 (m, 4H), 7.30−7.41 (m, 8H), 7.13−7.18 (m, 4H). ^{13}C NMR ($CDCl_3$) δ: 154.5, 146.7, 133.3, 132.0, 130.3, 129.8, 128.2, 127.7, 127.3, 126.7, 125.7, 107.3. IR (KBr disk) cm^{-1}: 1597. λ_{max} ($CHCl_3$) nm: 577. EI-MS: *m*/*z* 607. Anal. Calcd for $C_{32}H_{22}Br_3N_3$: C, 55.84; H, 3.22; N, 6.11. Found: C, 55.44; H, 3.19; N, 5.80.

[4-Bromo-5-(4-methoxyphenyl)-3-phenyl-1*H*-pyrrol-2-yl][4-bromo-5-(4-methoxyphenyl)-3-phenylpyrrol-2-ylidene]amine (17b). 16b (0.2 g, 0.392 mmol) was dissolved in dry benzene (15 mL) and treated with bromine (0.06 mL, 1.17 mmol) and the reaction stirred at room temperature for 2 h. The solvent was evaporated to dryness, yielding a black-green solid **17b** as the hydrobromide salt (0.28 g, 96%), mp 286−288 °C. ^{1}H NMR ($CDCl_3$) δ: 13.5 (bs, 2H), 8.31 (d, J = 8.8 Hz, 4H), 7.25−7.34 (m, 6H), 7.07−7.17 (m, 8H), 3.90 (s, 6H). ^{13}C NMR ($CDCl_3$) δ: 163.9, 154.1, 147.2, 134.3, 133.7, 131.0, 130.8, 129.2, 127.9, 119.5, 114.6, 108.1, 55.9. IR (KBr disk) cm^{-1}: 1604. λ_{max} ($CHCl_3$) nm: 600. EI-MS: *m*/*z* 667. Anal. Calcd for $C_{34}H_{26}Br_3N_3O_2$: C, 54.57; H, 3.50; N, 5.62. Found: C, 54.15; H, 3.22; N, 5.41.

[4-Bromo-3-(4-methoxyphenyl)-5-phenyl-1*H*-pyrrol-2-yl][4-bromo-3-(4-methoxyphenyl)-5-phenylpyrrol-2-ylidene]amine (17c). 16c (0.2 g, 0.39 mmol) was dissolved in dry benzene (20 mL) and treated with bromine (0.06 mL, 1.17 mmol) and the reaction stirred at room temperature for 2 h. The solvent was evaporated to dryness, yielding a blue-black solid **17c** as the hydrobromide salt (0.28 g, 96%), mp 306−307 °C. ^{1}H NMR ($CDCl_3$) δ: 14.04 (bs, 2H), 8.24−8.26 (m, 4H), 7.53−7.59 (m, 6H), 7.20−7.31 (m, 4H), 6.68 (d, J = 8.6 Hz, 4H), 3.85 (s, 6H). ^{13}C NMR ($CDCl_3$) δ: 159.9, 153.9, 146.1, 133.0, 131.7, 131.6, 130.2, 127.5, 125.9, 122.2, 112.1, 105.4, 54.2. IR (KBr disk) cm^{-1}: 1604. λ_{max} ($CHCl_3$) nm: 585. EI-MS: *m*/*z* 667. Anal. Calcd for $C_{34}H_{26}Br_3N_3O_2$: C, 54.57; H, 3.50; N, 5.62. Found: C, 54.17; H, 3.65; N, 5.25.

BF_2 Chelate of (3,5-Diphenyl-1*H*-pyrrol-2-yl)(3,5-diphenylpyrrol-2-ylidene)amine (18a). 16a (0.2 g, 0.45 mmol) was dissolved in dry CH_2Cl_2 (80 mL), treated with diisopropylethylamine (0.8 mL, 4.6 mmol) and boron trifluoride diethyl etherate (1 mL, 8.13 mmol), and stirred at room temperature under N_2 for 24 h. The mixture was washed with water (2 × 50 mL), and organic layer was dried over sodium sulfate and evaporated to dryness. Purification by column chromatography on silica eluting with CH_2Cl_2/hexane (1:1) gave the product **18a** as a metallic brown solid (0.19 g, 86%), mp 231−232 °C. ^{1}H NMR ($CDCl_3$) δ: 8.02−8.08 (m, 8H), 7.40−7.53 (m, 12H), 7.03 (s, 2H). ^{13}C NMR ($CDCl_3$) δ: 159.6, 145.7, 144.2, 132.4, 131.6, 130.9, 129.7, 129.6, 129.4, 128.7, 128.6, 119.2. IR (KBr disk) cm^{-1}: 1514. EI-MS: *m*/*z* 497.1. HRMS Calcd for $C_{32}H_{23}BF_2N_3$ [M + H]$^+$: 498.1953. Found: 498.1963. Anal. Calcd for $C_{32}H_{22}BF_2N_3$: C, 77.28; H, 4.46; N, 8.45. Found: C, 77.0; H, 4.38; N, 8.29.

BF_2 Chelate of [5-(4-Methoxyphenyl)-3-phenyl-1*H*-pyrrol-2-yl]-[5-(4-methoxyphenyl)-3-phenylpyrrol-2-ylidene]amine (18b). 16b (0.2 g, 0.39 mmol) was dissolved in dry CH_2Cl_2 (60 mL), treated with diisopropylethylamine (0.7 mL, 3.93 mmol) and boron trifluoride diethyl etherate (0.7 mL, 5.5 mmol), and stirred at room temperature under N_2 for 24 h. The mixture was washed with water (2 × 50 mL), and the organic layer was dried over sodium sulfate and evaporated to dryness. Purification by column chromatography on silica eluting with CH_2Cl_2/hexane (1:1) gave the product **18b** as a metallic red solid (0.16 g, 73%), mp 200−202 °C. ^{1}H NMR ($CDCl_3$) δ: 8.04−8.09 (m, 8H), 7.40−7.48 (m, 6H), 7.01−7.25 (m, 4H), 6.99 (s, 2H), 3.87 (s, 6H). ^{13}C NMR ($CDCl_3$) δ: 162.0, 158.1, 145.4, 143.1, 132.5, 131.8, 129.5, 129.4, 128.6, 124.2, 118.7, 114.3, 55.5. IR (KBr disk) cm^{-1}: 1600. EI-MS: *m*/*z* 557. HRMS Calcd for $C_{34}H_{27}BF_2N_3O_2$ [M + H]$^+$: 558.2164. Found: 558.2188. Anal. Calcd for $C_{34}H_{26}BF_2N_3O_2$: C, 73.26; H, 4.70; N, 7.54. Found: C, 73.16; H, 4.67; N, 7.45.

BF_2 Chelate of [3-(4-Methoxyphenyl)-5-phenyl-1*H*-pyrrol-2-yl]-[3-(4-methoxyphenyl)-5-phenylpyrrol-2-ylidene]amine (18c). 16c (0.13 g, 0.24 mmol) was dissolved in dry CH_2Cl_2 (30 mL), treated with diisopropylethylamine (0.41 mL, 2.41 mmol) and boron trifluoride diethyl etherate (0.41 mL, 3.37 mmol), and stirred at room temperature under N_2 for 24 h. The mixture was washed with water (2 × 50 mL), and the organic layer was dried over sodium sulfate and evaporated to dryness. Purification by column chromatography on silica eluting with CH_2Cl_2/hexane (1:1) gave the product **18c** as a metallic red solid (0.11 g, 88%), mp 288−290 °C. ^{1}H NMR ($CDCl_3$) δ: 8.05 (d, J = 8.9 Hz, 4H), 7.98−8.04 (m, 4H), 7.44−7.48 (m, 6H), 7.0 (d, J = 8.9 Hz, 4H), 6.92 (s, 2H), 3.90 (s, 6H). ^{13}C NMR ($CDCl_3$) δ: 161.0, 159.1, 145.5, 143.8, 131.9, 130.9, 130.6, 129.5, 128.5, 125.4, 117.5, 114.2, 55.5. IR (KBr disk) cm^{-1}: 1602. EI-MS: *m*/*z* 558.2. HRMS Calcd for $C_{34}H_{27}BF_2N_3O_2$ [M + H]$^+$: 558.2164. Found: 558.2174. Anal. Calcd for $C_{34}H_{26}BF_2N_3O_2$: C, 73.26; H, 4.70; N, 7.54. Found: C, 72.98; H, 4.62; N, 7.41.

BF_2 Chelate of [3-(4-Bromophenyl)-5-phenyl-1*H*-pyrrol-2-yl][3-(4-bromophenyl)-5-phenylpyrrol-2-ylidene]amine (18d). 16d (0.156 g, 0.26 mmol) was dissolved in dry CH_2Cl_2 (50 mL), treated with diisopropylethylamine (0.22 mL, 1.28 mmol) and boron trifluoride diethyl etherate (0.22 mL, 1.80 mmol), and stirred at room temperature under N_2 for 24 h. The mixture was washed with water (2 × 50 mL), and the organic layer was dried over sodium sulfate and evaporated to dryness. Purification by column chromatography on silica eluting with CH_2Cl_2/hexane (1:1) gave the product **18d** as a metallic brown solid (0.105 g, 62%), mp 265−266 °C. ^{1}H NMR ($CDCl_3$) δ: 8.04−8.07 (m, 4H), 7.93 (d, J = 8.3 Hz, 4H), 7.63 (d, J = 8.3 Hz, 4H), 7.51−7.53 (m, 6H), 7.06 (s, 2H). ^{13}C NMR ($CDCl_3$) δ: 159.9, 145.4, 142.9, 131.9, 131.3, 131.2, 130.6, 129.6, 128.7, 124.3, 119.3, 107.8. IR (KBr disk) cm^{-1}: 1519. EI-MS: *m*/*z* 654. HRMS Calcd for $C_{32}H_{21}BBr_2F_2N_3$ [M + H]$^+$: 654.0163. Found: 654.0190. Anal. Calcd for $C_{32}H_{20}BBr_2F_2N_3$: C, 58.67; H, 3.08; N, 6.41. Found: C, 58.40; H, 2.96; N, 6.23.

BF_2 Chelate of (4-Bromo-3,5-diphenyl-1*H*-pyrrol-2-yl)(4-bromo-3,5-diphenylpyrrol-2-ylidene)amine (19a). 17a·HBr (0.14 g, 0.20 mmol) was dissolved in dry CH_2Cl_2 (50 mL), treated with diisopropylethylamine (0.38 mL, 2.22 mmol) and boron trifluoride diethyl etherate (0.38 mL, 3.11 mmol), and stirred under N_2 for 24 h. The mixture was washed with water (2 × 25 mL), and the organic layer was dried over sodium sulfate and evaporated to dryness. Purification by column chromatography on silica eluting with CH_2Cl_2/hexane (2:1) gave the product **19a** as a metallic brown solid (0.12 g, 90%), mp 278−281 °C. ^{1}H NMR ($CDCl_3$) δ: 7.86−7.90 (m, 4H), 7.71−7.74 (m, 4H), 7.42−7.50 (m, 12H). ^{13}C NMR ($CDCl_3$) δ: 157.5, 143.3, 141.9, 129.8, 129.7, 129.5, 129.3, 128.6, 128.4, 127.0, 126.9, 109.8. IR (KBr disk) cm^{-1}: 1518. EI-MS: *m*/*z* 653. HRMS Calcd for $C_{32}H_{21}BBr_2F_2N_3$ [M + H]$^+$: 654.0163. Found: 654.0414. Anal. Calcd for $C_{32}H_{20}BBr_2F_2N_3$: C, 58.67; H, 3.08; N, 6.41. Found: C, 58.62; H, 3.04; N, 6.29.

BF_2 Chelate of [4-Bromo-5-(4-methoxyphenyl)-3-phenyl-1*H*-pyrrol-2-yl][4-bromo-5-(4-methoxyphenyl)-3-phenylpyrrol-2-ylidene]amine (19b). 17b·HBr (0.13 g, 0.174 mmol) was dissolved in dry CH_2Cl_2 (50 mL), treated with diisopropylethylamine (0.2 mL, 1.15 mmol) and boron trifluoride diethyl etherate (0.3 mL, 2.43 mmol), and stirred under N_2 for 24 h. The solution was washed with water (2 × 25 mL), and the organic layer was dried over sodium sulfate and evaporated to dryness. Purification by column chromatography on silica eluting with CH_2Cl_2/hexane (3:1) gave the product **19b** as a metallic brown solid (0.11 g, 88%), mp 271−273 °C. ^{1}H NMR ($CDCl_3$) δ: 7.84−7.87 (m, 4H), 7.75 (d, J = 9.0 Hz, 4H), 7.40−7.46 (m, 6H), 6.90 (d, J = 9.0 Hz, 4H), 3.85 (s, 6H). ^{13}C NMR ($CDCl_3$) δ: 161.7, 157.1, 144.0, 142.2, 132.7, 131.0, 130.9, 129.7, 128.2, 122.0, 113.8, 110.2, 55.5. IR (KBr disk) cm^{-1}: 1603. EI-MS: *m*/*z* 715. HRMS Calcd for

$C_{34}H_{25}BBr_2F_2N_3O_2$ $[M + H]^+$: 714.0375. Found: 714.0359. Anal. Calcd for $C_{34}H_{24}BBr_2F_2N_3O_2$: C, 57.10; H, 3.38; N, 5.88. Found: C, 57.30; H, 3.52; N, 5.87.

BF_2 Chelate of [4-Bromo-3-(4-methoxyphenyl)-5-phenyl-1*H*-pyrrol-2-yl][4-bromo-3-(4-methoxyphenyl)-5-phenylpyrrol-2-ylidene]amine (19c). 17c·HBr (0.18 g, 0.24 mmol) was dissolved in dry CH_2Cl_2 (100 mL), treated with diisopropylethylamine (0.30 mL, 1.72 mmol) and boron trifluoride diethyl etherate (0.30 mL, 2.44 mmol), and stirred under N_2 for 24 h. The solution was washed with water (2 × 25 mL), and the organic layer was dried over sodium sulfate and evaporated to dryness. Purification by column chromatography on silica eluting with CH_2Cl_2/hexane (1:1) gave the product **19c** as a metallic red solid (0.13 g, 76%), mp 297−298 °C. ^{1}H NMR ($CDCl_3$) δ: 7.91 (d, J = 8.7 Hz, 4H), 7.68−7.72 (m, 4H), 7.43−7.47 (m, 6H), 6.99 (d, J = 8.7 Hz, 4H), 3.89 (s, 6H). ^{13}C NMR ($CDCl_3$) δ: 159.9, 156.9, 143.1, 141.3, 131.4, 129.6, 129.2, 128.5, 126.9, 122.4, 112.6, 107.6, 54.3. IR (KBr disk) cm^{-1}: 1600. EI-MS: m/z $[M + H]^+$ 714. HRMS Calcd for $C_{34}H_{25}BBr_2F_2N_3O_2$ $[M + H]^+$: 714.0375. Found: 714.0352. Anal. Calcd for $C_{34}H_{24}BBr_2F_2N_3O_2$: C, 57.10; H, 3.38; N, 5.88. Found: C, 56.92; H, 3.33; N, 5.66.

Fluorescence Quantum Yield Measurements. Fluorescence quantum yields for **18a**−**d** and **19a**−**c** were determined in spectroscopic-grade chloroform at a concentration of 2×10^{-7} M. Mg-tetra-*tert*-butylphthalocyanine was used as a standard with a literature value for Φ_f of 0.84.[42]

Comparative Singlet-Oxygen Generation Measurements. An aerated 100 mL isopropyl alcohol solution of photosensitizer (5×10^{-6} or 5×10^{-8} M) and 1,3-diphenylisobenzofuran (5×10^{-5} M) was irradiated with a 250 W filtered red light source (>600 nm) at 25 °C for 1 h. Aliquots (2 mL) were removed from the reaction mixture at 5 min intervals, and a UV−visible spectrum was recorded. Reaction of 1,3-diphenylisobenzofuran with singlet oxygen was monitored by the reduction in intensity of the absorption band at 410 nm over time. Irradiation of a 100 mL isopropyl alcohol DPBF solution (5×10^{-5} M) in the absence of photosensitizer gave no reduction in intensity of the 410 nm absorption band over 1 h. Irradiation of a deoxygenated 100 mL isopropyl alcohol DPBF solution (5×10^{-5} M) containing either **18a** (5×10^{-6} M) or **19b** (5×10^{-8} M) gave no reduction in intensity of the 410 nm absorption band over 1 h.

Cytotoxicity Studies of 18a, 18b, 18c, and 19b. Stock photosensitizer solutions were diluted with minimum essential medium (MEM) containing 10% fetal calf serum (FCS). Cells were seeded at 5000 cells/well in 96-well plates and incubated for 24 h. Cells were incubated with photosensitizer in the dark for 3 h at 37 °C. The culture medium was removed, the cells were washed three times with PBS, and fresh culture medium was added to each well. The plates were irradiated with a light dose of either 8 or 16 J cm^{-2} from a filtered light source (wavelength 600−750 nm). Following irradiation, the cells were incubated for a further 48 h before being assessed for cell viability. The dark toxicity of each photosensitizer was also assessed in every experiment. Each assay was carried out in triplicate, and results are presented as an average.

Acknowledgment. This research was supported by grants from the Association for International Cancer Research, UK (AICR), and the Centre for Synthesis and Chemical Biology, University College Dublin, Ireland. Thanks to Dr. J. Gallagher for helpful crystallographic discussions, Dr. H. Mueller-Bunz of the UCD Crystallographic Centre and Dr. D. Rai of the CSCB Mass Spectrometry Centre for analysis.

Supporting Information Available: General experimental and experimental details for the synthesis of **14d** and **15a**−**d**; experimental details for CrEL formulation of **18a**−**d** and **19a**−**c**; cell culture, fluorescent microscopy, and confocal laser scanning microscopy methods; procedure for determining cytotoxicity of **1**; assay procedure for measurement of cell viability; UV−visible spectra for comparative singlet oxygen generation by **18a**; ^{1}H and ^{13}C NMR spectra for **16a**−**d**, **17a**−**c**, **18a**−**d**, **19a**−**c**; UV−visible for **16a**−**d**, **17a**−**c**, **18a**−**d**, **19a**−**c**; fluorescence spectra for **18a**−**d**, **19a**−**c**; X-ray crystallographic data of **19a** as a CIF file with a view of the crystal packing; complete focal plane CLSM image data for Figures 12 and 13 and movie of Figure 12. This material is available free of charge via the Internet at http://pubs.acs.org.

JA047649E

(42) Stiel, H.; Teuchner, K.; Paul, A.; Freyer, W.; Leupold, D. *J. Photochem. Photobiol. A* **1994**, *80*, 289.